to the starting model. The single thing in common among all travel time inversion schemes is that they are limited by the quality of the picks, and they are all subject to errors in geometry.

In this paper we discuss a method of displaying travel time data that provides a quick and effective quality control over survey geometry and pick quality. We also present a fast method of extracting an approximate slowness image directly from the picks. The method is equivalent to straight ray tomography, and has the simple interpretation of a radon transform of the pick space. Although these techniques cannot replace a thorough analysis and inversion of the data, they will complement any further analysis, and can, in principle, be performed very quickly in the field in order to get feedback on experiment quality.

QUALITY CONTROL OF EXPERIMENTAL GEOMETRY AND PICKED TIMES

A typical cross-well survey geometry is shown in Figure 1. A series of source positions lies within one well and a series of receiver positions lies in the second. Usually there is only one source tool and a small number of receivers. The receivers typically are held stationary while the source occupies many different depths; the receivers are then moved to a slightly different depth and the source again is swept through a range of depths. When the survey is complete, the data can be sorted into high fold common source gathers or "fans" and common receiver fans, as is often done with surface seismic reflection data.

A useful way to display the geometry is to plot shot depth vs. receiver depth as shown in Figure 2. Each dot represents a recorded trace, exactly as in a "stacking chart" for surface reflection data. All of the traces along any vertical line correspond to a common source fan, and all of the traces along any horizontal line correspond to a common receiver fan. Traces along lines at $+45°$ correspond to a common midpoint fan, which is less familiar in cross-well terminology. Similarly, traces along lines at $-45°$ correspond to common offset sections. When displayed this way, one can quickly see the fold, aperture dimensions, and variations of coverage with depth.

Traces from a typical high quality common receiver fan from an actual field experiment are shown in Figure 3, from which first arrival times were picked. A convenient way to display the times is by plotting them in the form of a colored stacking chart, as in Figure 4. For more sensitivity, the times plotted here are actually the differences relative to travel times in a uniform velocity medium, $\Delta t = t_{pick} - r/V_0$, where t_{pick} is the picked arrival time, r is the distance between the source and receiver, and V_0 is the uniform reference velocity. The positions of the colored dots in Figure 4a again show the survey geometry, as well as highlighting traces for which there are no picks. Figure 4b shows the same picks interpolated to make more clear the travel time patterns. One can immediately see systematic variations of residual travel time with depth, as well as with offset. Figure 4c shows the first attempt at creating the display in Figure 4b. The striking horizontal stripes show systematic shifts within

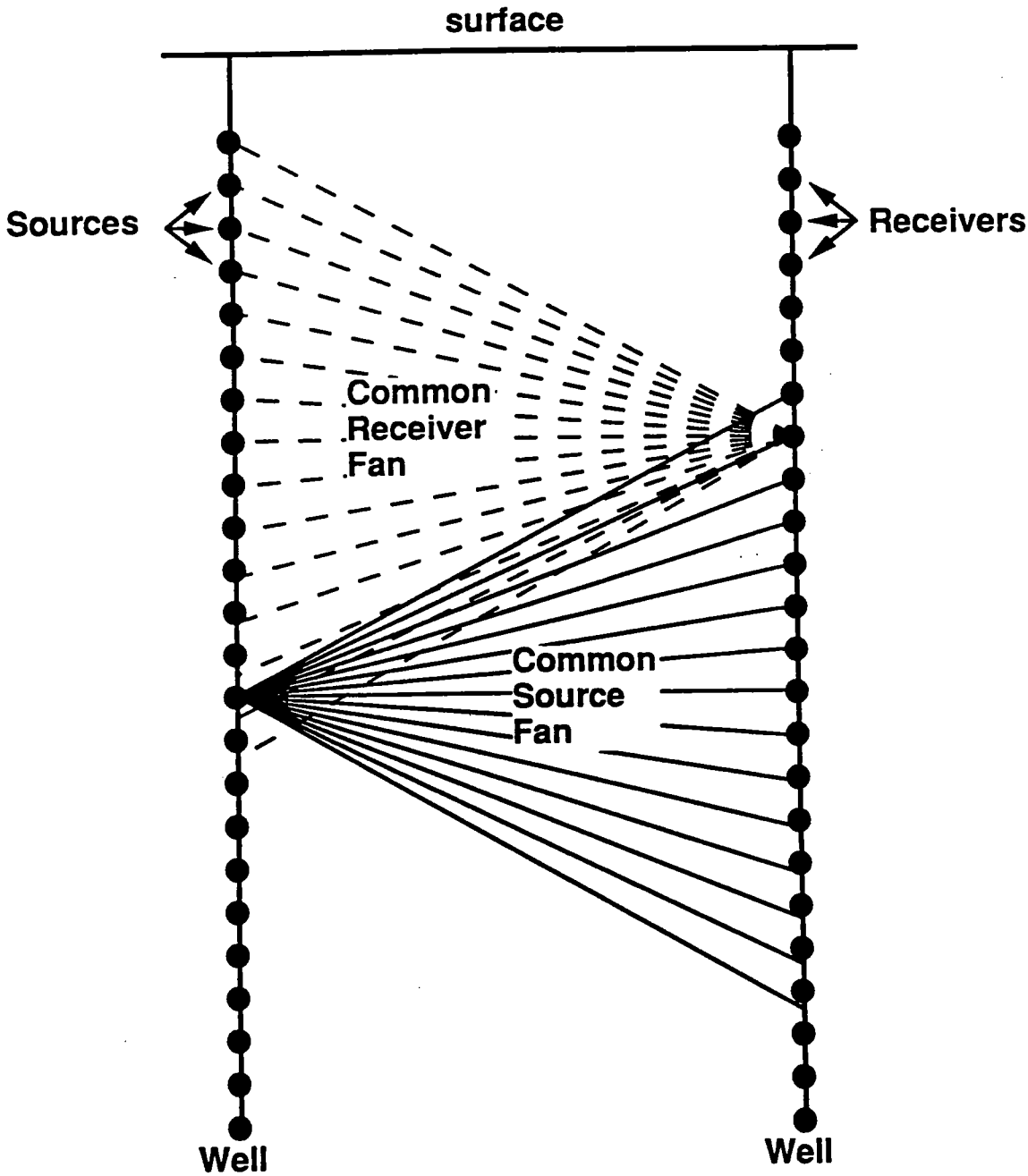

Figure 1: Typical crosswell survey. Sources lie in one well, receivers in the other. As with surface seismic data, traces can be sorted by common source, common receiver, common midpoint, or common offset.

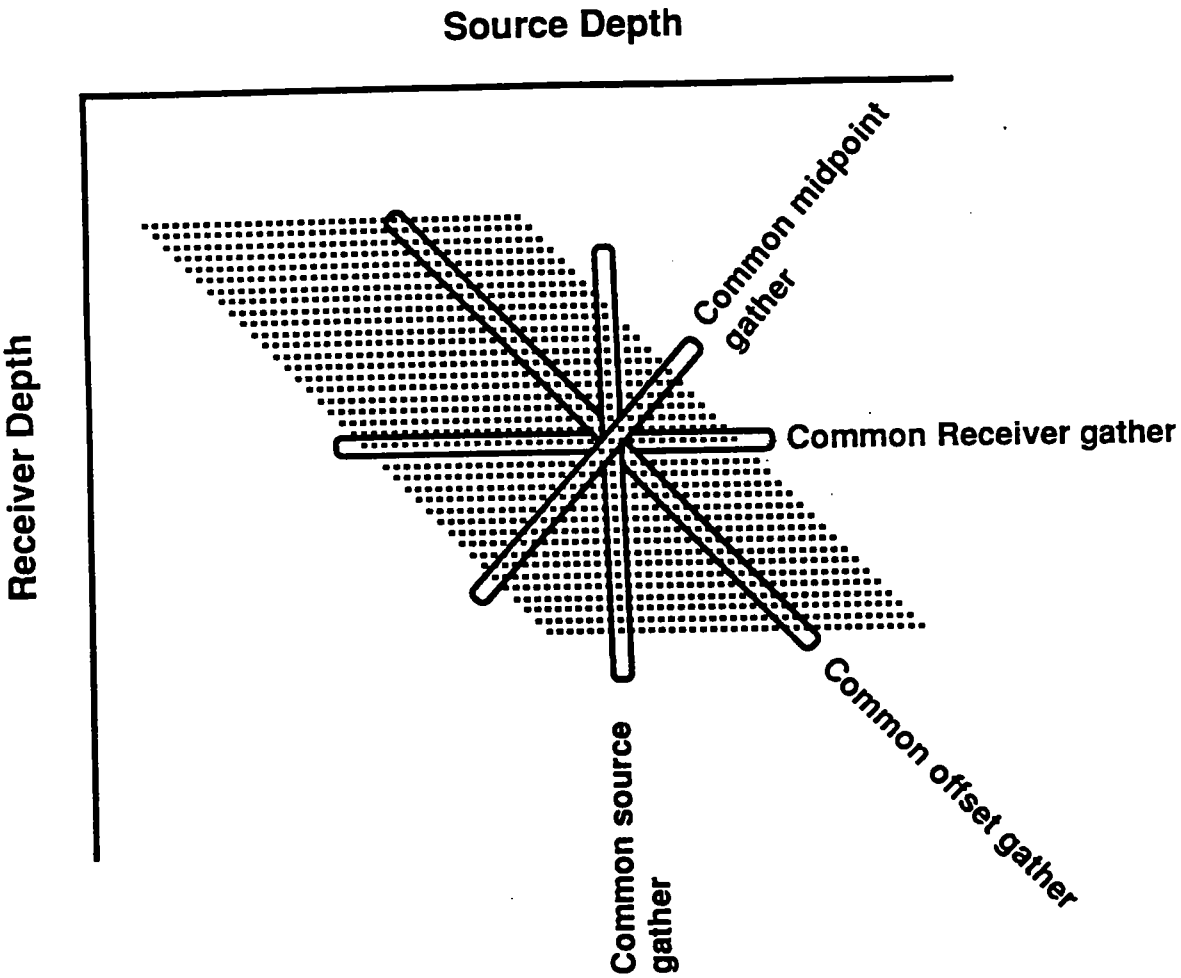

Figure 2: Stacking chart display of crosswell survey geometry.

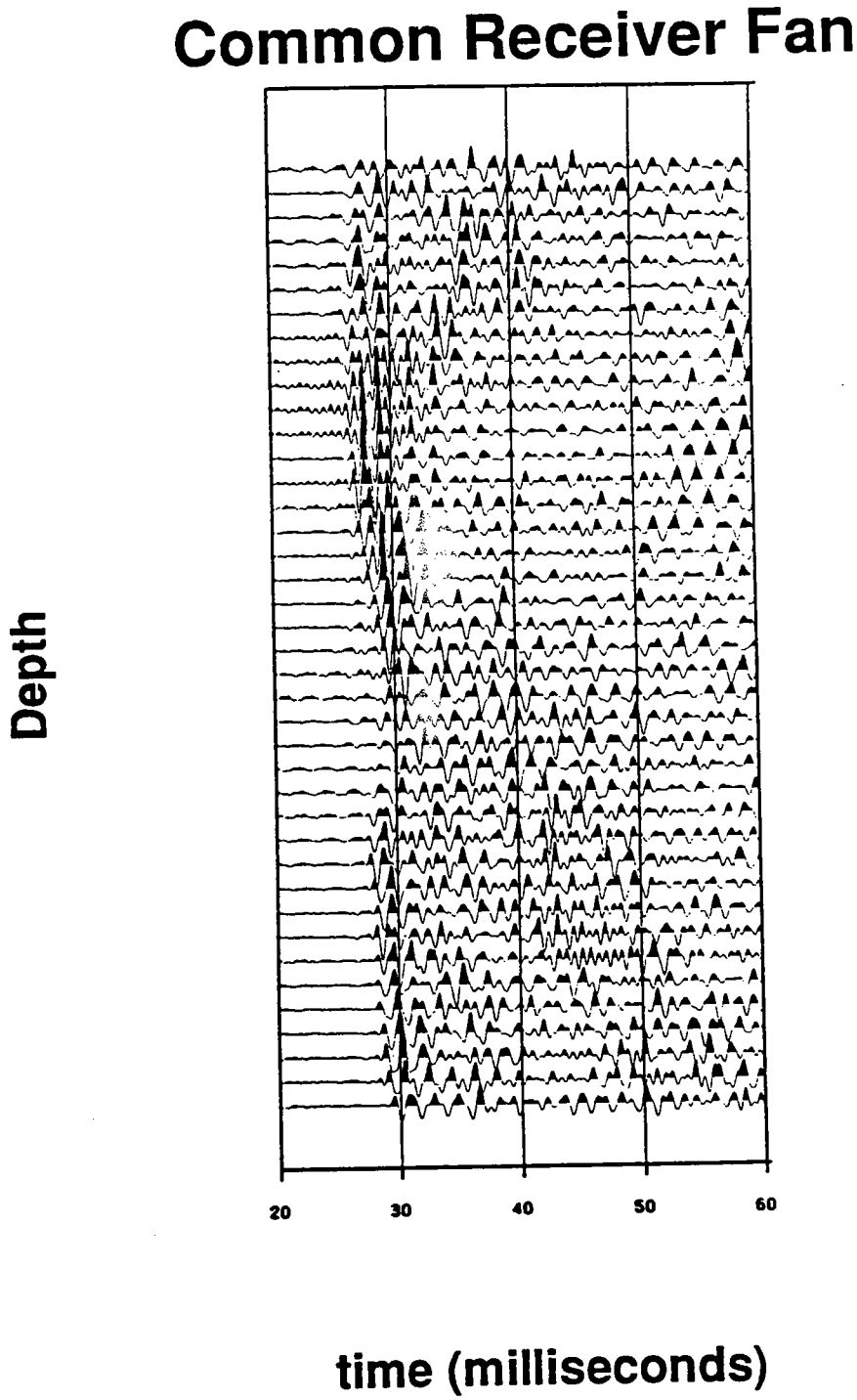

Figure 3: Near traces of a cross-well common receiver fan.

common receiver fans, that turned out to be a geometry error in extracting the receiver depths from the observer's logs. The unusual pattern was an immediate clue that something was wrong, and the horizontal nature indicated that it was systematically related to the receivers. The corrected display in Figure 4b shows very subtle horizontal streaks. The arrival times were picked by hand within common receiver fans; we suspect that occasional leg jumps were made when switching from one fan to the next, leading to slight receiver-consistent errors.

INTERPRETATION OF ARRIVAL TIMES

The travel time patterns in the corrected display, Figure 4b, directly indicate velocity variations in the formation between the wells. In general vertical streaks are related to a velocity anomaly near a source; horizontal streaks are related to an anomaly near a receiver, and streaks at other angles are related to anomalies between the source and receiver. One can also see the variation from slow to fast with depth. It would be useful if more detailed patterns can be recognized from these displays without the need for formal inversions. We explore this using synthetics.

Figure 5b shows a model which consists of 5 laterally uniform zero dip layers. Two wells are placed 100 meters apart. Sources are positioned every 4 m in the well on the left, between depths of 0 m and 400 m. Receivers are positioned every 4 m in the well on the right, between depths of 100 m and 300 m. Except at the top and bottom ends, each source is recorded by receivers ranging in depth from +/- 100 m of the source depth, and each receiver records sources ranging in depth from +/- 100 m of the receiver depth.

Rays were traced through the model to get travel times which we call the synthetic "picks". These are plotted in the stacking chart form in figure 5a, and have been divided by the straight line distance between source and receiver, to give them dimensions of slowness. The picks along the line $Z_{source} = Z_{receiver}$, which is the *zero offset* line, correspond to a cross-well log. Although rays may bend, this has the simple interpretation of horizontally propagating rays that sample the average slowness as a function of depth. The slownesses along this line agree very well with the model velocity vs. depth, as we expect. Other common offset gathers of picks give the average slowness between pairs of sources and receivers having a fixed vertical offset. The symmetric pattern of picks about the zero offset line indicates lateral symmetry in the model. The pattern of squares arranged along the zero offset line is characteristic of uniform flat layers; the square width is equal to the layer width. Although the synthetic rays were not straight, these patterns can be qualitatively compared with the Radon transform of simple slowness functions, as illustrated for example by Deans (1983).

A second model is shown in Figure 6b and consists of a single dipping fault separating two homogeneous layers. The source and receiver geometries are the same as before. The picks, converted to slowness, are plotted in Figure 6a. Again, the zero offset line shows the average slowness as a function of depth, which now has a

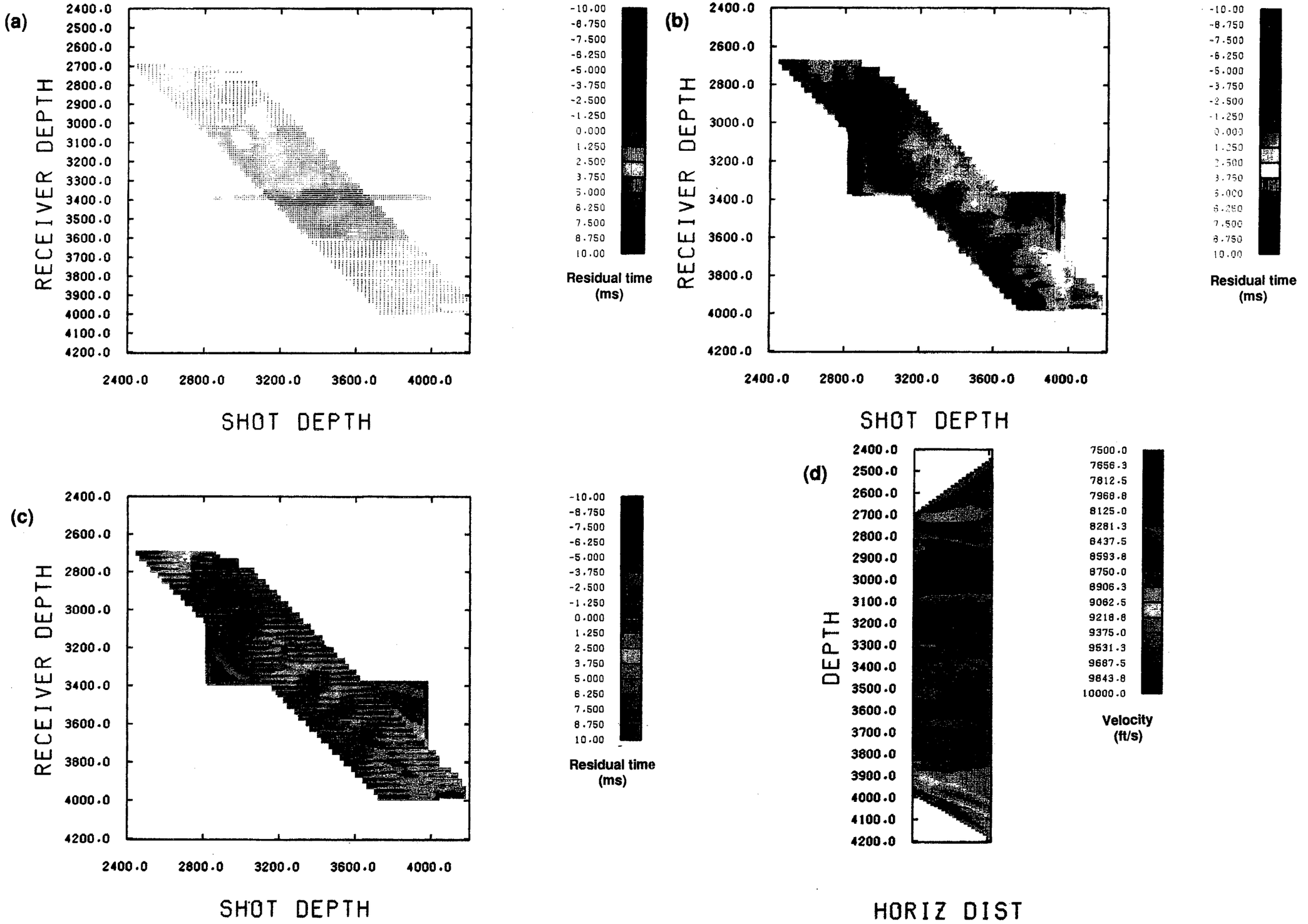

Figure 4: (a) Stacking chart display of crosswell survey trace attributes, in this case the picked first arrival times. Dot positions describe survey geometry; dot colors show residual travel times relative to an average velocity. (b) Residual travel times interpolated to better show the colored patterns of the travel time residuals. (c) Interpolated travel time residuals revealing a receiver-consistent geometry error. (d) Tomographic image obtained from the Radon transform of the picks in (b).

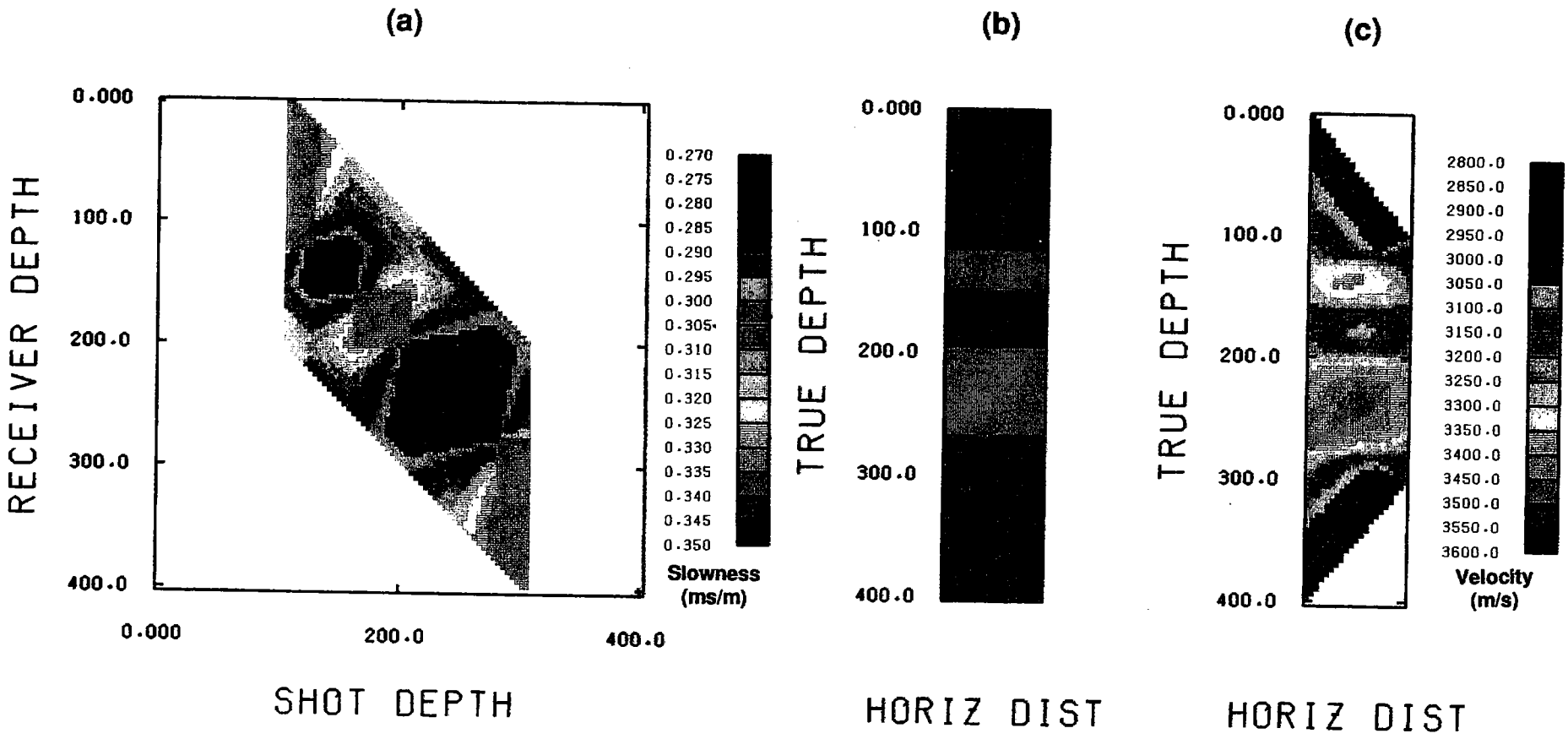

Figure 5: Flat layer synthetic study. (a) Picks converted to slowness obtained from curved rays traced through the model (b). (c) Image obtained from the Radon transform of the picks in (a)

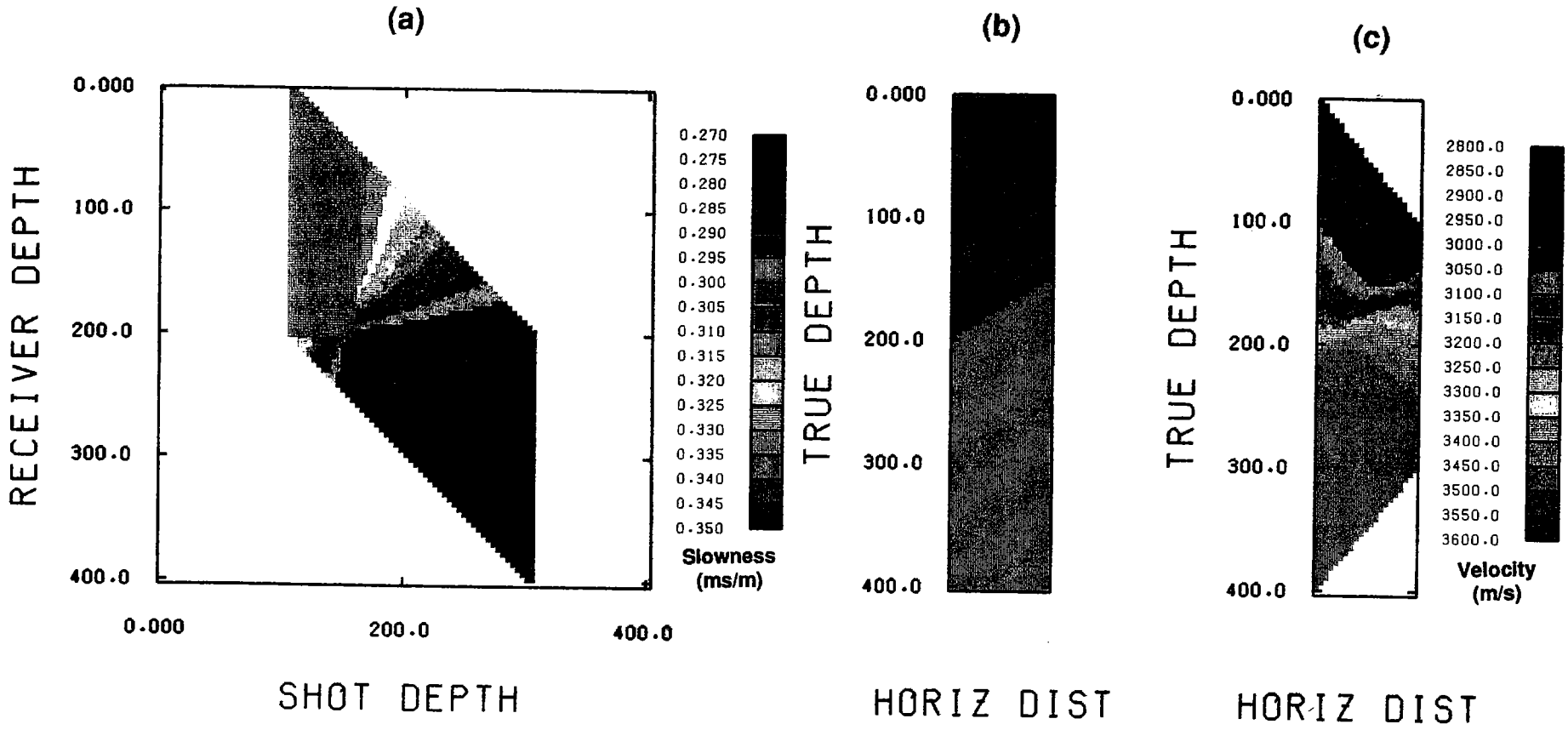

Figure 6: Faulted model synthetic study. (a) Picks. (b) Model. (c) Image obtained from the Radon transform.

gradient between depths of 150 m and 200 m which is the depth range spanned by the fault. Any lateral heterogeneity will tend to introduce gradients along the zero offset line. There is once again the pattern of squares, but it is offset because of the dipping fault. Since the pick domain plot is approximately the Radon transform of the model space, a rotation of the velocity boundary corresponds to a shift in the pick domain.

Our intuitive understanding of these patterns is based on averages of slowness along various ray paths. These interpretations have amounted to mentally inverting the Radon transform. We now discuss the process of more formally transforming the pick domain.

RAPID STRAIGHT RAY INVERSION IN THE PICK DOMAIN

Consider first a heurist arguement. As already discussed, all of the traces along any vertical line in the pick domain lie within a common source fan (Line A, in Figure 7a). These rays have in common the region immediately adjacent to the source at the well, and otherwise sample very different parts of the interwell region. One can imagine, then, that averaging all of these picks will tend to yield the near-source slowness and average out the variations away from the source. We therefore plot this average slowness at a point next to the source (point A in Figure 7b). Similarly, we imagine that averaging all of the picks along any horizontal line (line B in Figure 7a) gives the average slowness near the corresponding receiver, and we plot the average slowness at a point near the receiver (point B in Figure 7b). An average of the picks along a line at $+45°$ (line C in Figure 7a) represents the average of all straight rays passing though a particular mid point (point C in Figure 7b). Finally, all of the straight rays passing through a point at location (x, z) between the wells (point D in Figure 7b), lie along a line with angle $0° \leq \theta \leq 90°$ in the picks domain (line D in Figure 7a), where

$$\theta = tan^{-1}(\frac{X_0 - x}{X_0 + x})$$

and X_0 is the well spacing. This process of averaging is equivalent to taking a Radon transform of the pick domain. Each vertical line $x = constant$ in the image corresponds to one view of the transform.

Figures 4d, 5c, and 6c show the images that result from this process applied to the picks in Figures 4b, 5b and 6b, with slowness converted to velocities. It is clear that the Radon transform does a good job of estimating the various images. In each case the "inversion" took only seconds of cpu time on a Sun4 workstation.

We now discuss why this method works so well.

JUSTIFICATION OF THE INVERSION PROCEDURE

Each travel time measurement represents a line integral of the slowness along the raypath connecting source and receiver. For straight rays this is simply the Radon

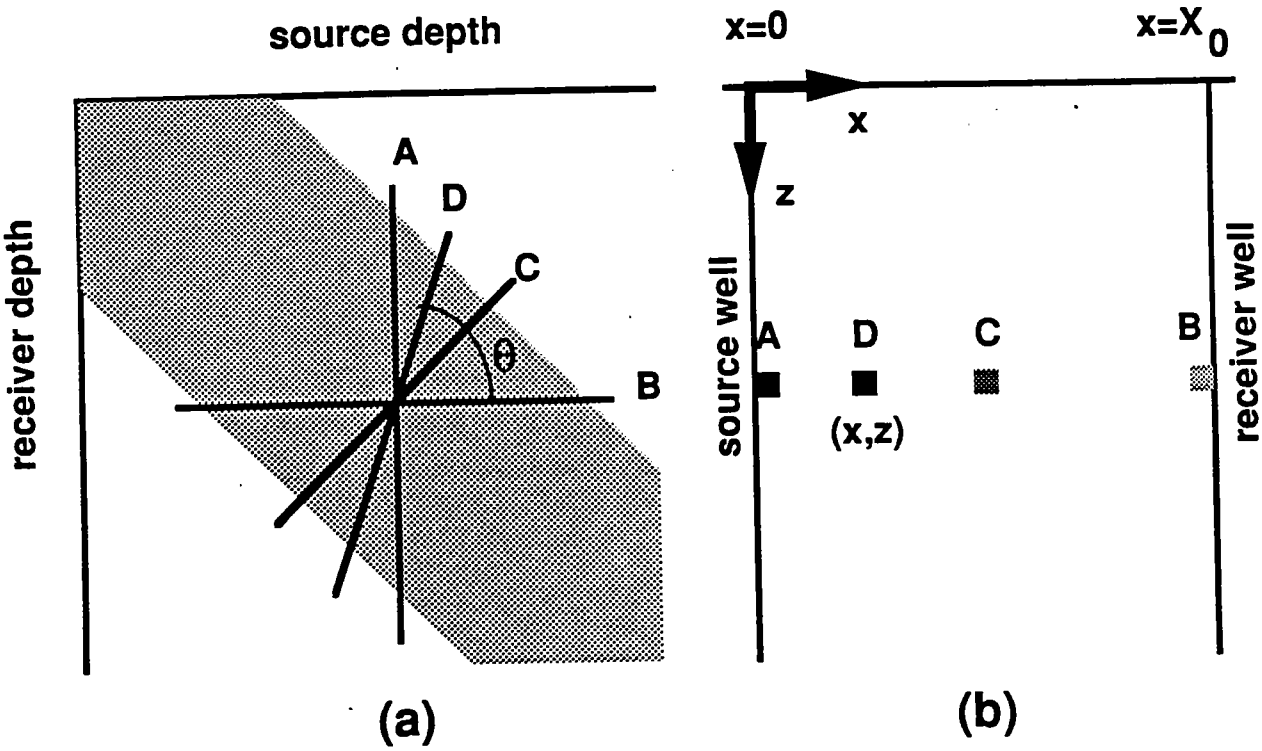

Figure 7: The imaging technique. Pick domain is shown on the left; space domain is shown on the right. Picks along **line** A (left) all pass through the **region** A (right), so the average of the slowness picks is plotted at **pixel** A. Similar for B, C, D, etc.

transform of the slowness and can be written formally as

$$t_\phi(l) = \int\int f(x,y)\delta(l - xsin\phi + zcos\phi)dxdz \tag{1}$$

where $\delta(l)$ is the Dirac delta function (Deans, 1983). The quantity t_ϕ is the travel time associated with a ray whose distance from the origin of the spatial coordinate system is $l = xsin\phi - zcos\phi$ and which forms an angle ϕ with the x axis. The two dimensional function $f(x,z)$ is the slowness that we wish to reconstruct.

The inverse of the Radon transform can be written formally as (Deans, 1983):

$$f(x,z) = -\frac{1}{4\pi}\int_0^{2\pi} \mathcal{H}\{\frac{dt_\phi}{dl}\}d\phi \tag{2}$$

$$= \frac{1}{\pi}\int_0^{\pi} t_\phi(l) * R(l)d\phi \tag{3}$$

where the operator $\mathcal{H}$ represents the Hilbert transform. The combination of the Hilbert transform and the derivative is known as the rho-filter, $R(l)$. We will demonstrate that our pick domain imaging scheme is a low frequency, discrete approximation of the exact inverse of the Radon transform. Unlike the familiar matrix inversion algorithms (ART,SIRT), it is not an iterative procedure. It is similar to the backprojection algorithms that are popular in medical imaging and radio astronomy. A good review of these techniques can be found in Lewitt (1983).

In the spatial frequency domain, the Radon transform inverse equation (3) can be written as

$$F(\rho,\theta) = \rho\hat{T}(\rho,\theta) \tag{4}$$

where ρ and θ are frequency domain polar coordinates, $F(\rho,\theta)$ is the two dimensional Fourier transform of the slowness image $f(x,z)$, and $\hat{T}(\rho,\theta)$ is the two dimensional Fourier transform of the unfiltered backprojection image $\hat{t}(x,z)$, defined as (Deans, 1983)

$$\hat{t}(x,z) = \frac{1}{\pi}\int_0^{\pi} t_\phi(l)d\phi \tag{5}$$

For a finite number of view angles, ϕ_i, $i = 1,2,...N$, equations (3) and (5) can be approximated as

$$f(x,z) = \frac{1}{\pi}\sum_{i=1}^{N} t_{\phi_i}(l) * R(l)\,\Delta\phi \approx \frac{1}{N}\sum_{i=1}^{N} t_{\phi_i}(l) * R(l) \tag{6}$$

$$\hat{t}(x,z) = \frac{1}{\pi}\sum_{i=1}^{N} t_{\phi_i}(l)\,\Delta\phi \approx \frac{1}{N}\sum_{i=1}^{N} t_{\phi_i}(l) \tag{7}$$

where $\Delta\phi = \pi/N$. Note that f has units of slowness and $\hat{t}$ has units of time. The difference between the images in equations (6) and (7) is the rho-filter, expressed as a one dimensional convolution of the individual views with $R(l)$ in the space domain, or multiplication with the spatial frequency ρ in the Fourier domain.

The rho-filter is the theoretically accurate way of transforming the time image $\hat{t}$ into the slowness image f. It accomplishes both a change of dimensions, by dividing by a length, and an enhancement of the high frequencies. However, the rho-filter is optimal for these purposes only when the rays are straight and when the projection angles ϕ_i range from 0 to π. With limited views and noisy data, a more conservative approach is to approximate the rho-filter with a filter $\tilde{R}(l) \approx R(l)$ that changes the dimensions of the projections to slowness with little or no boosting of the high frequencies. Our inversion method uses the simplest filter that accomplishes this, which is a constant $\tilde{R}(l) = \delta(l)/L_\phi$ where L_ϕ is the length of the ray path. The approximate image can then be written as:

$$f(x,z) \approx \frac{1}{N}\sum_{i=1}^{N} t_{\phi_i}(l) * \tilde{R}(l) \tag{8}$$

$$\approx \frac{1}{N}\sum_{i=1}^{N} t_{\phi_i}(l)/L_{\phi_i} \tag{9}$$

This filter converts each pick to the average slowness along the ray path, and its frequency response is flat. In practice, this is implemented by dividing each pick by the source-receiver distance, $L_\phi(l)$, which may be different for each ray, so it is not actually a convolution. For a very small finite number of views this gives a better estimate of the slowness image than using the rho-filter. For example, a single zero offset view will yield a laterally uniform image with the correct average slowness.

A different interpretation of our approximate method can be made in terms of direct Fourier reconstruction. The desired slowness image $f(x,z)$ can be written as

$$f(x,z) = \int_{-\infty}^{\infty}\int_{-\infty}^{\infty} F(k_x,k_z)e^{i2\pi(x\,k_x+(z\,k_z)}dk_x dk_z \tag{10}$$

$$= \int_{0}^{\pi}\int_{0}^{\infty} F(\rho,\theta)e^{i2\pi r\rho\,cos(\theta-\phi)}\rho d\rho d\theta \tag{11}$$

where F is the two dimensional Fourier transform of the slowness image expressed in either cartesian or polar coordinates. Polar coordinates are a natural choice for inverting tomographic data, because the travel times for each view determine spatial frequency components of the image that lie along a radial line (constant θ) in the frequency domain. A discrete approximation of the integral in equation (11) as a summation involves multiplying each measured Fourier component $F(\rho,\theta)$ by the polar coordinate element of 'area' $dA = \rho\, d\rho\, d\theta$, which has the effect of weighting high frequency (high ρ) measurements more than low frequency ones. This is equivalent to assuming that the unmeasured frequency components which lie between measured angles θ are equal to the nearest measured value at the same ρ. Our method instead weights all measured components equally by an element of 'area' $dA = d\rho\, dk_\perp$ where $dk_\perp$ is a tangential increment in the frequency domain. This resembles more a cartesian discrete fft of length M_{fft}, with local coordinates oriented parallel with a particular radial line θ, in which

$$dk_\perp = \frac{1}{M_{fft}\Delta s} \tag{12}$$

where Δs is the sample increment in the direction of the ray path. Then $M_{fft}\Delta s$ has the interpretation of the ray length L. In summary, the low frequency aspect of using the Radon transform as an inverse of the Radon transform can be viewed as a result of sampling the high frequencies less densely than the low frequencies, and reconstructing the image using only the measured Fourier components.

We have shown that except for the enhancement of high frequencies, our algorithm is an approximate one-step inversion of the Radon transform. If we ignore the rho-filter, the inversion extends naturally to the curved ray case. Hence, we can easily perform the same type of inversion in the real (x, z) space by back-projecting along the curved rays. This corresponds to a generalized Radon transform along curved trajectories in the pick domain. To implement the curved ray case requires knowing these curved trajectories.

CONCLUSIONS

We have presented a method of displaying cross-well seismic travel time data that provides a quick and effective quality control over survey geometry and pick quality. Times plotted in stacking chart form clearly show localized anomalies as linear streaks, which can be investigated as either geometry errors or true slowness anomalies. Other simple patterns corresponding to layers and faults can be qualitatively interpreted from published Radon transforms of simple functions. The method of display can obviously be extended to other trace attributes such as amplitude, pick quality, phase, or frequency.

We have also shown a very fast method of extracting an approximate slowness image directly from the pick domain. The operation is a Radon transform of the picks, and except for not enhancing the high frequencies, it is a one-step inversion of straight ray travel times. Although the method is not intended to replace a more thorough inversion of the data using curved rays, its speed and simplicity make it well suited for an initial assessment of the data. Such an imaging scheme might be incorporated, for example, into an interactive picking program, so that the image can evolve real time as picks are made. If performed in the field, the imaging can also give rapid feedback on the data acquisition.

The inversion method extends naturally to the curved ray case. Hence, we can easily perform the same type of inversion in the real (x, z) space by back-projecting the average slowness along the curved rays. This corresponds to a generalized Radon transform along curved trajectories in the pick domain. To implement the curved ray case requires knowing these curved trajectories, which is a topic of current study.

REFERENCES

Deans, S.R., 1983, The Radon Transform and Some of Its Applications, John Wiley & Sons, New York.

Devaney, A.J., 1984, Geophysical diffraction tomography, IEEE Trans. Geoscience

and Remote Sensing, GE-22, 3-13.

Harris, J.M., 1987, Diffraction tomography with arrays of discrete sources and receivers, IEEE Trans. Geoscience and Remote Sensing, GE-25, 448-455.

Justice, J.H., Vassiliou, A.A., Yale, D.P., and Lin., C.J., 1989, Rock properties and tomographic imaging in reservoir surveillance, 59th Ann. Internat. Mtg., Soc. Explor. Geophys., Expanded Abstracts, 760-762.

Justice, J.H., Vassiliou, A.A., Singh, S., Logel, J.D., Hansen, P.A., Hall, B.R.,Hutt, P.R., and Solanki, J.J., 1989, Acoustic tomography for monitoring enhanced oil recovery, The Leading Edge, 8, 2, 12-19.

Lewitt, R.M, 1983, Reconstruction algorithms: transform methods, Proceedings of the IEEE, 71, 3, 390-408.

Lines, L.R., and LaFehr, E.D., 1989, Tomographic modelling of a cross-borehole data set, Geophysics, 54,10, 1249-1257.

Lo, T-W., 1987, Seismic borehole tomography, Ph.D. dissertation, Massachusetts Institute of Technology.